A spatially resolved physical model for transient system analysis of high temperature fuel cells

CrossMark

Dustin McLarty, Jack Brouwer*, Scott Samuelsen

National Fuel Cell Research Center, University of California, Irvine, CA 92697, USA

ABSTRACT

This work builds upon previous high temperature fuel cell (HT-FC) modeling studies, capturing both steady state performance and transient behavior of HT-FC stacks by merging simplified dimensional aspects of a planar fuel cell stack with first principles physical modeling. Dynamic simulations are developed that spatially resolve fluctuations in temperature, pressure and concentration distributions during transient operation. A significant portion of the heat transfer occurs prior to and after the air passes over the electrochemically active portions of the cell, justifying additional heat transfer pathways from the stack to the air in order to accurately characterize the thermal transients and temperature distributions in the HT-FC stack. The highly configurable MatLab-Simulink® model developed can simulate both solid oxide and molten carbonate fuel cells utilizing either direct or indirect internal reforming. The perturbation response characteristics of the dynamic model to load, fuel flow, air flow and composition perturbations are discussed, and control strategies are introduced that minimize temperature fluctuations. Analysis indicates air flow and inlet temperature controls are sufficient to control average temperature and average internal temperature gradients. Internal heat transfer dynamics substantially change the spatial temperature distribution and local temperature gradients during typical operating conditions and perturbations.

Copyright © 2013, Hydrogen Energy Publications, LLC. Published by Elsevier Ltd. All rights reserved.

1. Introduction

The U.S. Department of Energy has devoted significant effort towards technological breakthroughs for highly efficient low emission electricity production [1–4]. Rising oil prices, the possibility of carbon taxation, and unnerving dependence on foreign energy sources stimulated the federal government's interest in clean energy sources that can meet new greenhouse gas emission targets. Fuel cells promise the dual benefits of high efficiency energy conversion and extremely low pollutant emissions, but adoption of the technology has been limited by high initial capital costs and lack of market acceptance. The challenges include poor economies of scale in manufacturing due to the relatively high materials costs and surface-area scaling characteristics, the complexity of the balance of plant and control systems, a lack of proven system durability, and operations and maintenance costs.

The combination of production advances and incentives have placed fuel cells on the cusp of widespread market adoption [5]. High temperature fuel cells have demonstrated remarkable performance in many stationary power applications [6–8]. Rapid market development and technological maturity requires a clear understanding of the underlying physics of operation and system integration complexities. The

	Nomenclature			
			T	Temperature
A_{Cell}	Cell Area		V	Volume
ASR_{eff}	Effective Area Specific Resistance		*Greek Letters*	
D_h	Hydraulic Diameter		α	Charge transfer coefficient
F	Faraday's Constant		η_{act}	Activation Polarization
FC	Fuel Cell		η_{conc}	Concentration Polarization
ΔG_{act}	Gibbs potential of Reaction		η_{cath}	Cathode Polarization
h	Convection Coefficient		η_{ohm}	Ohmic Polarization
j	Current Density		χ_i	Concentration of Species i
k	Conduction Coefficient		χ_{Cxx}	Concentration of Carbon Containing Molecules
$\dot{N}$	Flow Rate		χ_{H2xx}	Concentration of H_2 Containing Molecules
n_{cell}	# of Cells In Stack		*Subscripts*	
P	Pressure		A	Anode
PEN	Positive electrode, Electrolyte, Negative electrode		C	Cathode
R	Rate of Reaction		in	Inlet
R_U	Universal Gas Constant		out	Outlet
R	Recirculation			

electrochemical physics are well understood. However, significant gaps in understanding still exist for systems integration and design before most HT-FC systems can be effectively deployed. Integration challenges can be addressed with detailed physical models that are capable of accurately capturing and predicting system responses to forced operational perturbations and fluctuations in ambient conditions. This work aims to develop a dynamic fuel cell stack model that incorporates these features and apply the model to a simple system for perturbation response and control analyses.

2. Background

Molten carbonate fuel cells (MCFC) typically consist of a high temperature (550–650 °C) molten salt electrolyte sandwiched between nickel electrodes, producing moderately high current densities of 0.1–.25A/cm². Molten carbonate fuel cells have operated on methane, biogas [9], and syngas [10], utilizing either internal or external steam reformation and water-gas shift [11–13]. Sheng et al. demonstrated sensitivity to small changes in peak temperature and temperature gradients despite high operating temperatures. Excessive peak temperatures and gradients within a fuel cell can lead to rapid degradation, physical fatigue and failure [14]. Mitigation of thermal fluctuations can be achieved with a cascade control strategy for optimal electrical production during load fluctuations [15]. However, the inability of most commercial MCFC systems to measure internal stack temperature distributions limits the applicability of this strategy. MCFC models in the literature typically utilize bulk parameters for increased computational efficiency, sacrificing the accuracy that could otherwise be obtained using a spatially resolved model [16,17]. Brouwer et al. compared overpotential terms derived from the Nernst equation to those of an agglomerate model. The agglomerate model approach represented the operating voltage at low current densities more effectively [16].

Solid oxide fuel cells (SOFC) are typically comprised of a yttria-stabilized zirconia electrolyte, and either ceramic,

metallic, or composite electrodes [18]. High temperature SOFC have demonstrated fuel flexibility with operation on hydrogen, natural gas, and coal derived syngas [19–21]. The solid state SOFC technology offers attractive features for a wide range of applications including small distributed power generation, future large grid-connected power generation, and auxiliary power plants aboard naval, land and aerospace vehicles [22–25]. Several potential applications require rapid transient load following capability, a historical weakness of fuel cell systems [26]. The work of Mueller et al. investigated three different mechanisms that contribute to SOFC transient behavior at multiple time scales. Electrochemistry responds on the order of milliseconds, air and fuel propagation occurs within a few seconds, and thermal transients last minutes to hours, depending upon the thermal mass of the stack. Experiments conducted with an operating SOFC short stack have demonstrated the fuel flexibility and internal reforming characteristics of SOFC technology [22].

3. Model description

In the current work, a spatially- and temporally-resolved fuel cell model has been developed using the MatLab᷇Simulink® interface. The model, derived from first principles, incorporates the necessary physics for both MCFC and SOFC simulations. A generic planar cell design with scalable geometric dimensions and variable spatial resolution is simulated with direct and indirect internal reforming, Fig. 1. Simulation of any spatial resolution is readily accomplished by specifying
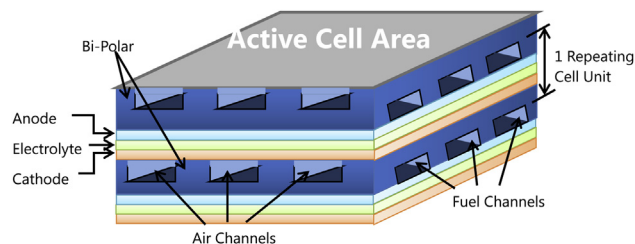

Fig. 1 – Planar fuel cell repeating unit.

the number of rows and columns during the model initialization. Various air and fuel flow directions can be specified including co-flow, counter-flow, and cross-flow patterns. Indirect internal reformation occurs within unique cells spaced periodically within the stack arrangement. Previous dynamic models of both SOFC and MCFC technologies have developed controls for basic load following operation, but have not captured the spatial resolution or internal heat transfer necessary to resolve spatial temperature gradients [27,28].

Reformation kinetics, described by Achenbach, applies within the anode channels and reformation plates [29]. If the system utilizes an external reformer the kinetic rate constants of Xu and Froment are applied to a spatially discretized reformer model with an appropriate catalyst loading factor specific to the materials set [11]. The analysis presented considers bulk (single node), linear (20 node), and quasi-3-D (120 node) models capable of co-flow, counter flow and cross flow simulations. A sensitivity study of spatial resolution, omitted for brevity, demonstrated diminishing benefit with additional computational cost beyond 10 nodes in the primary air flow direction. The design of the current model applies to a variety of planar fuel cell designs and readily scales to various cell dimensions and stack heights. The simplified geometry incorporates all of the relevant physical features and behavior of both MCFC and SOFC technology.

Dynamic modeling with one or two degrees of spatial resolution allows for analysis of the internal temperature profile behavior, the distribution of reformation and electrochemistry, and internal flow and concentration transients. Internal reformation, which depends upon local species concentrations, temperature and catalyst loading, and local reactant consumption determine downstream concentrations, local heat generation and current density. The current distribution is resolved by imposing an equipotential constraint across all of the nodes for the voltage difference between anode and cathode. This method ensures that the voltage of the cell responds realistically (and does not vary across the electrode) by solving for the current distribution at each time step. The approach provides significant improvement in accuracy over a bulk model, particularly in the tasks of scaling, control, and determining precise physical operation and transient limits. Bulk model parameters are tuned for a particular cell, and don't effectively scale with dimensional parameters since heat transfer and mass transport properties remain fixed. Bulk models provide minimal insights into specific performance limits such as physical stresses or spatial variations of temperature, species concentrations and current density.

A spatially resolved modeling methodology suitable to this study of performance, integration and control of high
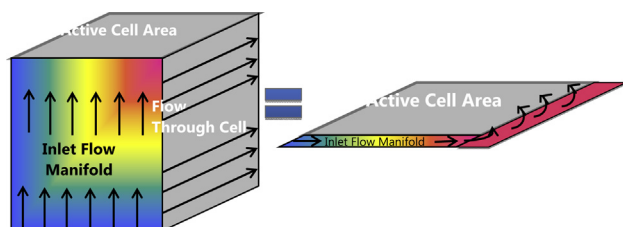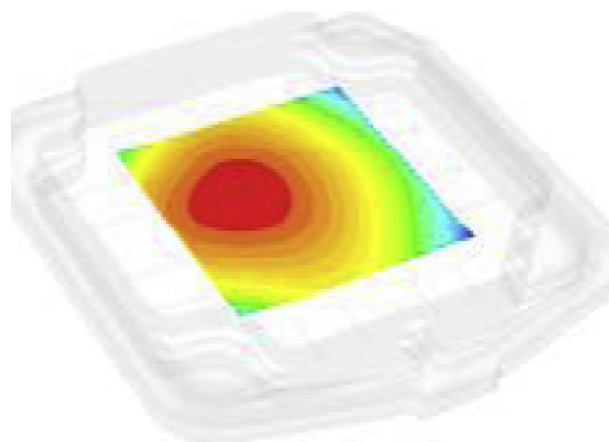

Fig. 3 – FCE spatial temperature profile [31].

temperature fuel cells has been previously developed at the University of California, Irvine and applied to integrated high temperature fuel cell systems [16,26] and fuel cell - gas turbine hybrid systems [30–32]. The methodology discretizes the fuel cell into five distinct control volumes in the transverse direction; anode current collector, anode gas channels, positive electrode-electrolyte-negative electrode (PEN), cathode gas channels, and cathode current collector, as shown in Fig. 1. Within each volume the temperature, species concentrations, pressure, voltage and current density are evaluated with dynamic conservation of mass, energy and momentum equations, as required. Models of additional energy system components such as heat exchangers, external reformers, combustors and turbo-machinery are typically integrated with these spatially resolved fuel cell models to form complex models of integrated energy systems that incorporate the resolution of individual system component physics, chemistry and electrochemistry as needed. Simultaneous solutions of relevant dynamic expressions capture the complex and coupled interactions amongst system components.

The current work extends the previous methodology into a quasi-3-D representation of co-flow, cross-flow or counter-

Fig. 2 – Conceptual view of geometric simplification (3-D to Quasi 3-D).
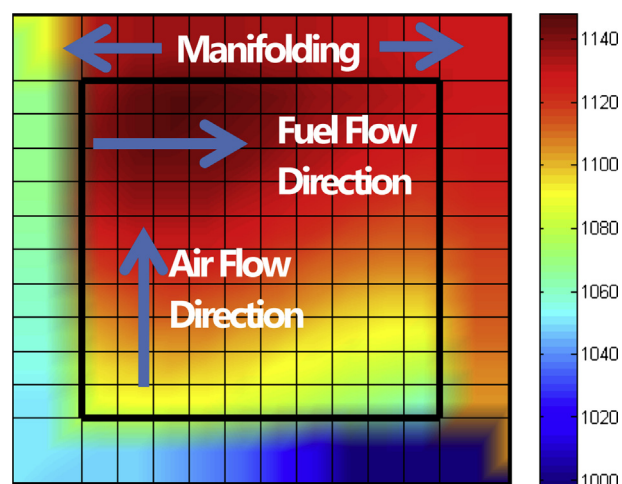

Fig. 4 – Current model temperature profile (with manifold physics).

flow geometry fuel cells, with integration of pre- and post-cell heating manifolds into the stack configuration, representing a novel modeling approach of reduced stack geometry, as shown in Fig. 2. This innovation captures the heat transfer that couples the fuel and air manifold with cell performance and temperature distributions of a 3-dimensional stack. This achievement extends from a simplification of the manifold geometry wherein the incoming air and fuel streams flow across the cell edges in the stack prior to entering and after exiting the active cell area. Fig. 3 shows a steady state cross flow temperature distribution from Fuel Cell Energy [33]. Fig. 4 compares that to a profile generated by the novel model developed in this study. The spatially resolved temperature profiles clearly demonstrate similar thermal behavior, temperature gradients and local temperature distribution within the active cell area.

The modeled inlet flow configuration along the cell edges does not physically represent the air flow path of the integrated fuel cell stack configuration, but this method allows for energy transfer directly from the stack to the incoming air and fuel streams in a computationally efficient manner that well simulates the actual heat transfer that occurs in the manifolds and the impacts of this heat transfer on cell temperature distributions. The goal for this geometric simplification is to accurately capture important thermodynamic coupling under dynamic conditions, which is justified by the following qualitative evidence:

- Thermal energy generated by electrochemical reactions in the cell preheats the inlet air and fuel streams in the manifolds (between 25 °C and 50 °C temperature rise is common in real stacks at full load conditions [34–37].
- The final cathode exhaust stream temperature closely mirrors that of the peak PEN temperature, and is not the source of energy for internal pre-heating.
- The spatial temperature profile of the PEN closely matches that of Fuel Cell Energy's cross flow cell model.
- Internal (to the cell) flow advects any internally generated heat toward the exhaust stream due to low Peclet numbers; thus, upstream energy mobility exists only in the solid cell stack components; tri-layer and interconnects. High convective and radiative heat transfer to the inlet manifolds results in conduction limited heat transfer from the solid portions of the fuel cell. Therefore internal temperature profiles are independent of manifold geometry and depend solely on edge areas and conductive heat transfer coefficients.

The spatial temperature profiles presented in Figs. 3 and 4 represent the SECA target goals for the SOFC case of 100 °C temperature rise, 500 mW/cm^2 power density, and a fuel utilization of 80% [38,39]. This method captures the extremely important coupling effect of operating power density and internal pre-heating. With constant air flow, additional power/heat generation will differentially increase operating temperature, temperature gradients and air pre-heating depending upon the precise cell and air flow geometry. Variable air flow systems meet additional power/heat generation with additional cooling air to maintain constant operating temperature, though internal temperature distributions may vary.

Table 1 – Fuel cell reaction vectors.

HT-FC	Molten carbonate	Solid oxide
$R_{Cathode}$	$\left[\, 00 \quad \dfrac{-1 \cdot i}{2F} \quad 000 \quad \dfrac{-1 \cdot i}{4F} \,\right]$	$\left[\, 000000 \quad \dfrac{-1 \cdot i}{4F} \,\right]$
R_{Anode}	$\left[\, 00 \quad \dfrac{1i}{2F} \quad \dfrac{-1 \cdot i}{2F} \quad \dfrac{1 \cdot i}{2F} \quad 00 \,\right]$	$\left[\, 000 \quad \dfrac{-1 \cdot i}{2F} \quad \dfrac{i}{2F} \quad 00 \,\right]$

A typical variable air flow control strategy maintains fixed cathode inlet and outlet temperatures and presumes that the cell temperature gradients remain constant. The internal temperature distribution during operation and the associated stack performance, thermal stress, and degradation cannot be resolved without spatial resolution of the physics we are discussing.

Spatial modeling reveals the coupling of manifold heat transfer to other cell performance characteristics, for example, how additional air flow increases internal temperature gradients through reduced air pre-heating and a redistributed temperature profile. A controller that incorporates variable cathode inlet temperature and variable air flow, by manipulating both blower speed and a recirculation valve, can address this challenge and substantially reduce fluctuations of internal temperature gradients during dynamic operation. Incorporating feedback from internal temperature sensors into the controllers would allow for additional perturbation response. The important coupled response of internal pre-heating and temperature gradient to air flow and power output must be captured in dynamic analyses and control studies. The strategy employed in this study is a novel simplified method of simulating the interaction between air flow rate and internal pre-heating in cell stack manifolds under dynamic operating conditions.

4. Model development

The models of varying spatial resolution developed in this study incorporate the following expressions to account for electrochemistry; conservation of mass and energy; species concentrations; and heat and mass transfer within and between each control volume. Dynamic conservation equation (1), applies to each gaseous control volume. The expression assumes a perfectly stirred reactor with the exit conditions representing the concentrations throughout the control volume.

$$\frac{R_{REF} + R_{USE} + (\dot{N}\chi)_{in} - (\dot{N}\chi)_{out}}{\dfrac{P_j V_j}{R_U T_j}} = \frac{d\chi_i}{dt} \tag{1}$$

The reaction rates, Table 1, for the cathode and anode gases are based upon the appropriate half reactions on each electrode of a molten carbonate or solid oxide fuel cell. The electrochemical (R_{USE}) and chemical (R_{REF}) reaction rates are arranged in a vector comprised of the seven species considered throughout the fuel cell, [CH$_4$ CO CO$_2$ H$_2$ H$_2$O N$_2$ O$_2$]. A positive reaction rate indicates production while a negative rate indicates consumption. The fuel utilization is calculated from the fuel flow rate and current as a ratio of the hydrogen

available from the fuel and methane reformation and the hydrogen consumed by electrochemical reactions. The hydrogen consumption, equation (3), is proportional to the current density, j, multiplied by the area of the cell, A_{cell}, and the number of cells in the stack, n_{cell}. Fuel flow can be controlled, based upon the current or upon the power, to be either constant fuel utilization or constant heating.

$$Util_{fuel} = \frac{H_{2,consumed}}{H_{2,available}} \qquad (2)$$

$$H_{2,consume} = \frac{n_{cell} \cdot j \cdot A_{Cell}}{2 \cdot F} \qquad (3)$$

$$H_{2,avail} = \dot{n}_{fuel} * \left(4 \cdot \chi_{CH_4} + \chi_{CO} + \chi_{H_2}\right) \qquad (4)$$

Similarly, air utilization is calculated as the ratio of oxygen consumed to that supplied. Air flow may be fixed, variable, or controlled through a recirculation loop. Advanced controller strategies may incorporate thermocouple measurements of stack inlet, exhaust, or internal temperatures in addition to the standard voltage and current measurements. Higher air utilization, for a fixed power and temperature gradient, suggests a more efficient fuel cell that requires less cooling air. At high air utilization the partial pressure of oxygen diminishes in downstream portions of the cells, starving the fuel cell of oxygen, and increasing the polarization losses.

Methane reformation and water gas shift chemistry calculations, are calculated on the basis of the well-established kinetic reaction mechanism outlined by Achenbach et al. [29]. These authors outlined three reactions involved in the production of hydrogen from methane and water, and measured the rate parameters associated with each of the following reactions.

$$CH_4 + H_2O \rightarrow CO + 3H_2 \qquad (5)$$

$$CO + \tfrac{1}{2}O_2 \rightarrow CO_2 + H_2O \qquad (6)$$

$$CH_4 + 2H_2O \rightarrow CO_2 + 4H_2 \qquad (7)$$

Reformation occurs in the anode compartment as a function of pressure, temperature, and species concentrations. The presence of catalyst material on the anode surface also plays a role in the reformation kinetics and local heat transfer. The concentration and distribution of the catalyst can influence the location of the endothermic reformation and is therefore incorporated as a means of controlling spatial temperature in the typical cell design. Counter-intuitively, the catalyst loading should be lower at the entrance of the cell to extend the reformation to downstream portions of the cell and avoid inlet freezing from excessive reformation reactions near the fuel inlet. An alternative to internal reformation within the anode compartment itself is the deployment of separate reformer plates within the stack specifically used for reformation. In the Fuel Cell Energy DFC® design such reformer plates are placed between every 10 cells, or so, and can be approximated in the current model using appropriate boundary conditions for conduction heat transfer from the top and bottom of the fuel cell (to the reformer plates). The rate of reactions in the reformer is determined as follows using the kinetic mechanism discussed above.

$$R_{REFORM} = f(P, T, \chi_{out}) \qquad (8)$$

Conservation of energy and conductive, convective, and radiative heat transfer apply throughout and between each of the control volumes resulting in a detailed heat transfer model capable of well simulating the fuel cell temperature distribution. Local conditions and material properties are used to estimate conduction between and amongst the three solid layers. Convection, assuming fully-developed flow, estimates the heat transfer between the solid layers and gaseous flows. The indirect internal reforming design includes a non-electrochemically active reformer cell designed to be directly inserted between every ten electrochemically active cells in the stack. The reformer cell acts as a heat sink due to the endothermic reforming chemical reactions, providing a significant portion of the internal stack cooling. Table 2 presents several intrinsic and extrinsic properties of the stack, anode, cathode, and electrolyte material properties that complete the physical description of the FC model developed in the current study. Each parameter can be modified to calibrate the model to any particular fuel cell design.

The molten carbonate voltage calculations use expressions for three typical classes of loss terms: activation, Ohmic and concentration losses. The Butler—Volmer equation, the fundamental equation of electrochemical kinetics, is used to characterize activation polarization. The simpler Tafel expression (equation (9)) approximates the Butler—Volmer equation at moderate to high current densities. The charge transfer coefficient, α, can range between 0 and 1 depending upon the specific system. The area specific resistance, ASR_{eff}, that is multiplied by local current density, j, to determine the Ohmic losses is calibrated to empirical tests performed at the University of California Irvine [16,40].

$$\eta_{act} = -\frac{RT}{\alpha nF}\ln j_0 + \frac{RT}{\alpha nF}\ln j \qquad (9)$$

Table 2 — Fuel cell parameters.				
Component	Parameter	Unit	MCFC	SOFC
Stack	Length	m	1.2	0.25
	Width	m	0.8	0.25
Bipolar Plate	Thickness	m	0.02	0.006
	Density	kg/m^3	7900	1975
	Specific Heat	J/kg-K	611	611
	Conductivity	W/m-K	25.4	25.23
Anode	Channel Height	m	0.004	0.002
	Channel Width	m	0.004	0.005
	Wall Thickness	m	0.005	0.002
Cathode	Wall Thickness	m	0.005	0.002
	Channel Height	m	0.006	0.002
	Channel Width	m	0.006	0.005
Electrolyte	Membrane Thickness	m	0.001	18e-6
	Cathode Thickness	m	N/A	800e-6
	Anode Thickness	m	N/A	50e-6
	Density	kg/m^3	2702	375
	Specific Heat	J/kg-K	1146	800
	Conductivity	W/m-K	218	6.19
Reformer	Channel Height	m	0.005	N/A
	Channel Width	m	0.003	N/A
	Wall Thickness	m	0.001	N/A

$$ASR_{eff} = C_2 + C_1 * T \tag{10}$$

$$\eta_{ohm} = j \cdot ASR_{eff} \tag{11}$$

Concentration losses arise from the diffusion limitations of reactant gases to the reaction sites and product gases from the reaction sites. Production of electrical current requires continual supply (replenishment) of reactants to the triple phase boundary (TPB); however, the rate of reactant replenishment is limited by diffusion through the electrode. The reactant concentrations at the TPB affect the fuel cell performance through the Nernst potential and through the reaction kinetics. These mechanisms are summarized in an expression for the net concentration loss using the local current density, j, limiting current density, j_L, bulk-stream and TPB reactant concentrations, c_R.

$$\eta_{cath} = \frac{R_U T}{4F} \ln \frac{j \cdot c_R^*}{j_L \cdot c_R^0} \tag{12}$$

The ratio of species concentration between the bulk-steam, c_R^0, and TPB, c_R^*, can be defined in terms of the local pressure P^C, free stream oxidant concentration, X_{O_2}, cathode thickness, t^C, local current density, j, and effective cathode diffusivity, D^{eff}.

$$\frac{c_R^*}{c_R^0} = \frac{1}{P^C \left\{ x_{O_2|d} - t^C j RT / \left(4FP^C D_{O_2,N_2}^{eff} \right) \right\}} \tag{13}$$

Having accounted for both activation and concentration losses with the previous expression, all that remains to be found is the Ohmic loss. The SOFC Ohmic resistance is calculated using area specific resistance, ASR, and the local current density, j, and area, A. ASR depends upon membrane thickness, t^M, electrolyte temperature, T, and reaction potential, ΔG_{act}.

$$\eta_{ohm} = j * \frac{t^M T}{A_{cell} e^{-\Delta G_{act}/(RT)}} \tag{14}$$

Calculation of local convective heat transfer assumes fully developed flow and uniform surface temperature within each control volume. An approximate Nusselt number of four, determined from standard engineering tables, was used with equation (15) to calculate local convection using conductivity, k, and hydraulic diameter, D_h, of the channel.

$$Nu_D = \frac{h D_h}{k} \tag{15}$$

The composition of the cathode inlet stream plays a significant role in the overall performance of the cell. A reduction in oxidant concentration at the cell inlet reduces oxidant partial pressure throughout the cell. This negatively impacts the local Nernst potential and loss terms, thereby producing more heat and reducing the efficiency of the cell. Cathode recirculation, if present, can increase or decrease the oxidant concentration at the inlet. Cathode recirculation diminishes oxygen concentration when diluting ambient air, but increases CO_2 concentration which provides a counter-benefit of increasing the other electrochemically active oxidant species in the case of an MCFC.

A molten carbonate fuel cell recycles CO_2 from the anode compartment and post combustor into the cathode inlet stream. The anode off-gas is diluted with atmospheric air, and

the resulting inlet species can be found with equations (16)–(19). The solid oxide model employs ambient air containing only oxygen and nitrogen as an oxidant stream. The re-circulated gas stream will also primarily consist of oxygen and nitrogen with slightly lower oxygen content. equations (20) and (21) represent the expressions for the inlet species concentrations of the SOFC cathode.

$$X_{CO_2} = \frac{\{\dot{n} X_{C_{XX}}\}_{A,out} + R(\dot{n} X_{CO_2})_{C,out}}{\{\dot{n}\}_{C,in}} \tag{16}$$

$$X_{H_2O} = \frac{(\dot{n} X_{H_{2XX}})_{A,out} + R(\dot{n} X_{H_2O})_{C,out}}{\{\dot{n}\}_{C,in}} \tag{17}$$

$$X_{O_2} = \{X_{O_2}\}_{Air} \left(1 - \frac{\{\dot{n}(1 + 2X_{CH_4})\}_{A,out}}{\{\dot{n}\}_{C,in}} \right) \tag{18}$$

$$X_{N_2} = 1 - X_{O_2} - X_{H_2O} - X_{CO_2} \tag{19}$$

$$X_{O_2} = (1 - R)\{X_{O_2}\}_{Air} + R\{X_{O_2}\}_{C,out} \tag{20}$$

$$X_{N_2} = 1 - X_{O_2} \tag{21}$$

5. Steady state performance results

Initial model testing and verification relied on a parametric variation of key design parameters including fuel utilization, average operating temperature, PEN temperature gradient, and power density. Results were consistent with previous studies, but the spatial resolution and novel integration of the fuel and air manifold in the current model offered additional insights into temperature profile variation with power density and the system and cell level thermal response to various operating conditions [8,16,19,20,33]. The MCFC model was also used to investigate the impact of CO_2 concentration and steam-to-carbon ratio on system performance. The results demonstrate the robustness of the novel model design for simulating relevant physical phenomena.

Fig. 5 illustrates the difference in steady state internal temperature distribution for a variety of cell conditions including air flow direction, the presence on internal reformation, and the edge cooling provided by the fuel and air
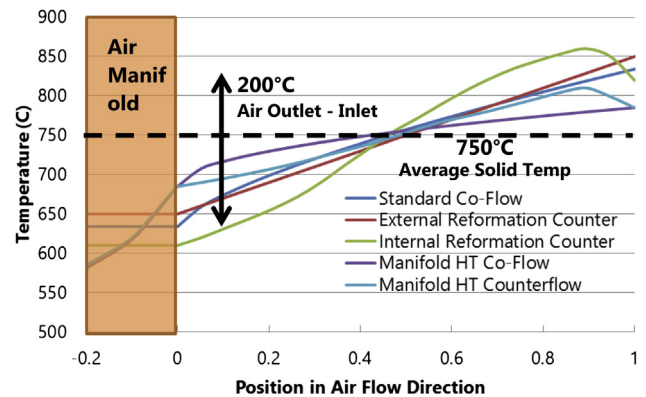
Fig. 5 – Internal temperature profiles for different model configurations.

manifold of the stack. Each variation was constrained to identical conditions of average temperature and average thermal gradient, though the resulting temperature profiles are substantially different. Counter flow, air and fuel flowing in opposite directions, with partial internal reformation resulted in the highest thermal gradients within the cell. Similar internal temperature profiles are demonstrated in the work of Aguiar et al. for a co-flow SOFC with internal reforming [41]. This analysis demonstrates similar transient modeling capability but considers several additional flow geometries, quasi-3-D spatial resolution and the additional heat transfer pathway between the stack and the air manifolding.

Key insights into performance characteristics that are not apparent through study of the governing equations and standard V–I characteristics are gained. Several of these attributes may have little bearing on a stand-alone FC system, but can significantly alter or be used for control of an integrated FC system when coupled with a gas turbine. The data presented results from simulation using the quasi-3D model in a cross-flow configuration. Similar results have been obtained for the counter-flow configuration, which demonstrate that the temperature profile and current distribution are the primary differences between the flow configurations. The current parametric analysis was conducted with a voltage controller used to converge to the desired power density. A second air flow controller adjusted the rate of oxidant supply to achieve the desired cathode heating. A final controller actuating a recirculation valve adjusted the temperature of the cathode inlet streams to maintain a fixed average PEN temperature. Twenty-nine system parameters were recorded and analyzed for each operating condition.

Variation of fuel utilization, the proportion of available hydrogen consumed in the fuel cell, was found to significantly impact cell performance. Fig. 6 demonstrates the positive impact on system efficiency with increasing fuel to air ratio and fuel utilization. Lower fuel utilization produces higher hydrogen concentrations throughout the anode compartment, reducing activation and diffusion losses and raising the fuel to air ratio. When losses are reduced, the air flow requirement decreases, simultaneously raising both cell efficiency and reducing the need for cooling air flow (and corresponding blower parasitic power). Though the cell operates more efficiently, the unspent fuel is converted only to heat thus decreasing the system efficiency unless anode recirculation
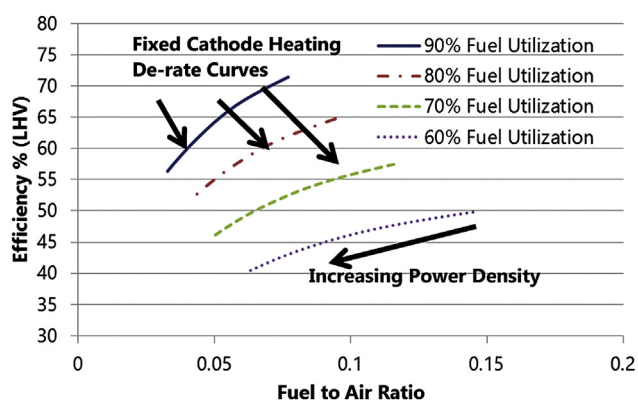
or a hybrid cycle is employed. Lower current operation reduces Ohmic losses thereby also increasing the cell efficiency and fuel to air ratio, but without the associated system penalty of unused fuel. MCFC systems exhibit an additional benefit of higher inlet CO_2 concentration at higher fuel to air ratios, resulting in optimal fuel utilizations that are lower than those for SOFC systems. The extremely low current density regime is not shown due to numerical solution difficulty at high oxidant utilization factors when air flow is reduced to maintain the desired temperature gradient. The high current regime is not depicted due to the existence of multiple solutions for current and voltage resulting in the same power density. Controlling voltage rather than power allows lower voltage operating conditions to be investigated.

The model employed demonstrates the novel capability of capturing the coupled effects of air flow rate, power density and internal heating by capturing the physics of stack air and fuel delivery in manifolds, as discussed previously. The air flow rate into the FC is controlled to obtain a 200 °C temperature rise from inlet to outlet, thus as the PEN temperature gradient decreases the temperature rise in the manifold increases. The amount of pre-heating achieved by the heat exchange in the manifolds is not constant, and will be reduced with increasing air flow. Many factors including fuel utilization, cell temperature gradient, and power density affect the flow rate of cooling air needed to maintain a fixed cell operating temperature. These factors are found to have little effect on the ratio of internal (across the active cell area) vs. external (in the manifolds) pre-heating. Simulating a broad range of operating conditions and plotting them on a logarithmic scale, Fig. 7, demonstrates that air flow largely dictates the ratio of internal temperature rise (across the active cell area to external pre-heating. The two distinct linear slopes on the logarithmic plot indicate a difference in the limiting heating process between low and high air flow rates. At low air flow rates the convective heat transfer is low, but the mass of air to pre-heat is small and the residence time in the manifolds and heat exchangers is longer. Thus the pre-heating can reach a temperature closer to the operating cell temperature and the cell edges are nearly as warm as the center, resulting in an even temperature distribution with little thermal stress. At higher flow rates the residence time is shorter and the amount of air to heat significantly greater, thus a lower temperature is reached despite a higher heat transfer rate. The higher air flow
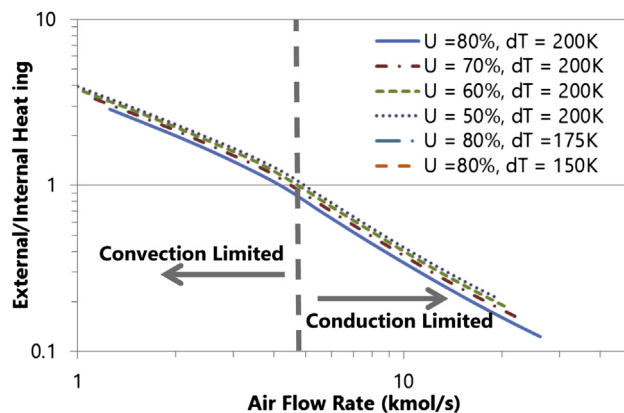

Fig. 6 – SOFC efficiency vs. Fuel to air ratio.

Fig. 7 – Log–log plot of heating ratio vs. Air flow rate.

increases the convective heat transfer until the cell edges are cooled and the internal conduction can match the necessary heat transfer to the incoming air. This results in an increased temperature gradient across the cell that is necessary to conduct heat from where it is generated by the electrochemistry to where it pre-heats the incoming air. Designs with thicker tri-layers, and greater heat conduction to and through the interconnects can mitigate the rise in thermal gradients, thereby extending the convection limited regime to higher air flow rate regimes.

Fig. 8 shows the need for substantial reduction in air flow rate during turndown beyond that needed to maintain a fixed cathode inlet temperature. Fig. 8 indicates that in order to maintain a fixed operating temperature and temperature gradient within the cell, the stack inlet temperature should decrease substantially at part-load, by as much as an additional 50% reduction in air flow. This reduction in air flow rate beyond that which would maintain fixed cathode inlet temperature, is the counter-intuitive means by which one can maintain stack temperature distributions with the variable pre-heating that occurs in the inlet air manifolds. This control concept deviates substantially from controls presented in the literature [41–43] and those used in present systems which primarily control air flow rate in proportion to current [44,45].

As the model suggests, the cell temperature profile dependence observed is due solely to the cell materials, flow geometry, and the coupled air flow manifold heat transfer impacts on conduction and convection heat transfer in the stack. An electrochemical model is not necessary to predict the characteristic pre-heating of any particular design, but, this important finding that could not have been elucidated without the new cell model concept. Detailed spatial resolution and capture of the manifold pre-heat physics are necessary to capture this behavior. The amount by which the preheating would vary for different air flow rates that is required to appropriately control the internal temperature distribution during turndown cannot be determined without such an approach. This study presents a dynamic simulation of such a control scenario which maintains internal temperature gradients during a large turn-down transient.

The temperature distribution and peak thermal gradient within a fuel cell depends upon three operational parameters: power density, fuel utilization, and stack temperature rise. Steep temperature gradients and thermal oscillations play substantial roles in several degradation mechanisms. Maintaining a constant temperature profile during transient
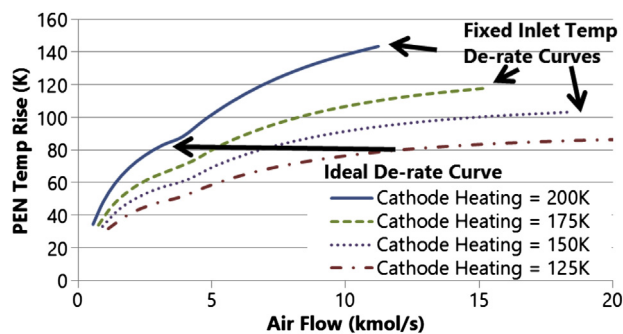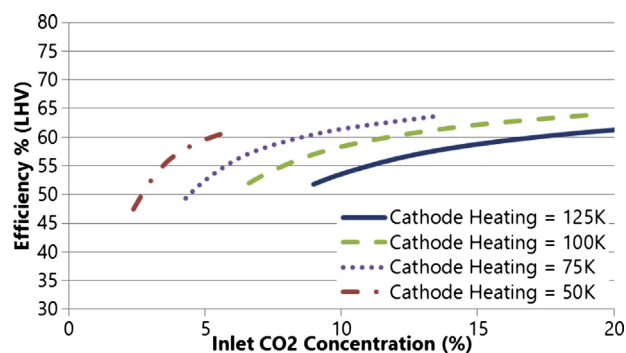
Fig. 9 – MCFC efficiency vs. inlet CO_2 concentration.

operation can vastly improve the longevity of the fuel cell [14]. The widely employed method of controlling only stack inlet and exhaust temperature could allow substantial temperature variations during transient and off-design operation. This study supports the development of additional control systems that can affect thermal gradients of various cell geometries to minimize degradation and fracture due to thermal stress when operating over a broader range of load conditions.

The carbon dioxide inlet concentration and steam-to-carbon ratio studies presented in Fig. 9 relate only to MCFC. Carbon dioxide concentration depends upon the anode off-gas composition and the amount added to ambient air for systems that incorporate anode off-gas recycle as the CO_2 source for the cathode inlet stream. The expressions for calculating inlet composition were presented in the model development section. Cathode recirculation can supply additional CO_2 for FC-GT hybrids, with recirculation requirements determined by pre-heating and turbine temperature requirements. Fig. 9 demonstrates the positive impact of higher CO_2 inlet concentrations on carbonate cell and system efficiency. Additionally it can be seen that a higher fuel to air ratio, resulting from a greater cathode heating rate, also increases the CO_2 composition and thereby the efficiency. The rise in efficiency reduces the cooling requirement, further increasing the fuel to air ratio and system efficiency. This positive feedback mechanism can also be reversed, demonstrating how a slightly less efficient cell or operating condition necessitating higher air flow rates can result in reduced CO_2 concentration and further reduced efficiency.

The benefit of re-circulating more CO_2 is reduced as CO_2 concentration increases (diminishing returns) thus providing a limit to the gains in efficiency. The additional heat capacity of CO_2 reduces cooling requirements, as does the reduced heat generation from more efficient operation stemming from a greater diffusion of CO_2 to the reactant sites; a potential boon to hybrid systems, whose performance depends heavily on the amount of cooling air. In systems without cathode recirculation there is a direct relationship between fuel to air ratio and inlet CO_2 concentration in MCFC. This relationship can be exploited in hybrid systems by operating at lower fuel utilizations to boost the fuel to air ratio, and also in co-generation systems producing usable hydrogen as a byproduct [46].

Some studies suggest controlling the steam ratio as a means of temperature control for MCFC systems [12,17]. This study supports these claims, demonstrating a slight reduction
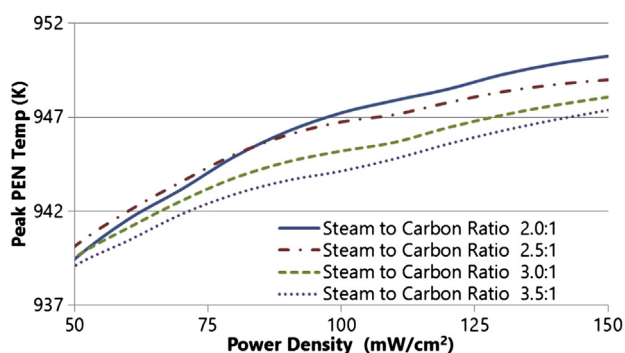
Fig. 8 – SOFC solid temperature gradient vs. flow rate with fixed inlet temperature control.

Fig. 10 – MCFC peak temperature vs. power density and steam to carbon ratio.

Table 4 – Solid oxide overpotential parameters.

Physical property	Variable	Value	Units
Effective Oxygen Diffusivity	D_{O_2,N_2}^{eff}	2×10^{-5}	(m^2/s)
Transfer Coefficient	α	0.7	(none)
Exchange Current Density	j_o	1	(A/cm^2)
Electrolyte Constant	A	13×10^7	(K/Ω^*m)
Electrolyte Activation Energy	ΔG_{act}	100	(kJ/mol)
Electrolyte Thickness	t^M	18	μm
Anode Thickness	t^A	50	μm
Cathode Thickness	t^C	800	Mm

in peak electrolyte temperature at higher steam concentrations. The cathode gas stream still accounts for most of the stack cooling, but the increasing steam concentration reduces the high current region near the fuel entrance that produces the highest temperature anywhere in the cell. The increased steam also promotes a more complete reformation of the methane feedstock, producing more hydrogen and raising overall cell voltage. This effect diminishes above a steam-to-carbon ratio of 3.0 when near complete methane reformation occurs.

Fig. 10 presents data with varying steam-to-carbon fuel ratios. A slight reduction in voltage occurs as the steam-to-carbon ratio increases from 2 to 3.5, but efficiency may be sacrificed in order to mitigate the increase in the peak cell temperature by as much as 30%. Higher steam-to-carbon ratios reduce the likelihood of coking, but eventually become detrimental to performance as the partial pressure of fuel is diminished. This study indicates a peak steam-to-carbon ratio of approximately 3.0. Additionally, water in the fuel stream increases thermal capacitance of the anode gas coupled with increased internal reformation. Water-gas shift provides additional stack cooling. The primary reason for the reduction in peak temperature is reduction of localized peak temperature near the fuel entrance. High temperatures occur in this high current density region due to high local fuel concentrations. Thermal gradients away from the edges depend upon the material thickness and thermal conductivity properties of the PEN and interconnects.

calculations. This enables the study of different control strategies for temperature management of integrated HT-FC systems. The analysis described herein presents open-loop (uncontrolled) FC dynamic responses to four different perturbations: power demand (which corresponds most immediately to cell voltage changes), fuel flow rate, air flow rate, and fuel composition, as a means of verifying the dynamic model prior to implementing system level control strategies. The response analysis generated insights into the relative magnitude and time scale of different perturbation impacts and indicated which perturbations induced responses that were outside of operational limits or those that required specific control strategies to mitigate. Each study began from a design case with parameters and operating conditions as listed in Tables 2–5.

The first perturbation, a step change in power demand (corresponding to a step change in voltage from 695 mV to 655 mV), causes a sudden rise in current density as the lower voltage allows the cell to rapidly consume the hydrogen present in the anode compartment. In less than 1 s the additional hydrogen consumption has reduced the partial pressure of hydrogen, increased the diffusion losses, and settled at a new current density only slightly higher than the original. The fuel utilization has increased and, coupled with the decreased voltage, has given rise to significantly more internal heat generation. This in turn raises the operating temperature of the fuel cell, a transient that occurs on the order of 100 s, as shown in Fig. 11. The rising temperature reduces Ohmic losses; gradually raising the current and power output. The system eventually reaches a new equilibrium when the increase in power output reduces the heat available for pre-heating the incoming air sufficiently to maintain a constant operating

6. Dynamic results

The model described in this paper was derived and implemented in the Matlab-Simulink® interface for dynamic

Table 3 – Voltage loss parameters for MCFC.

Physical property	Variable	Value	Units
Limiting Current Density	j_l	4000	Amps/m²
Curve Fit Term 1	C_1	6.667×10^{-7}	Ohm–m²/K
Curve Fit Term 2	C_2	4.783×10^{-4}	Ohm–m²
Charge Transfer Coefficient	α	0.4	none
Exchange Current Density	j_o	50	Amps/m²

Table 5 – Fuel cell parameters.

Parameter	Case 1	Case 2	Units
Power Density	500	200	mW/cm²
Voltage	0.8685	0.9702	Volts
Current	316.64	113.34	Amps
Fuel Utilization	80%	80%	
Fuel Species	[0.0049 0.0262 0.0378 0.91 0.0001 0.021 0 0.149]	Same	
Oxidant Species	[0 0 0 0 0 0.81 0.19]	Same	
Fuel Flow	0.149	0.0536	kmol/s
Air Flow	7.391	1.8329	kmol/s
PEN T_{avg}	1023	1023	K
Cathode T_{in}	875.67	840.7	K
Cathode T_{out}	1054.7	1039.1	K

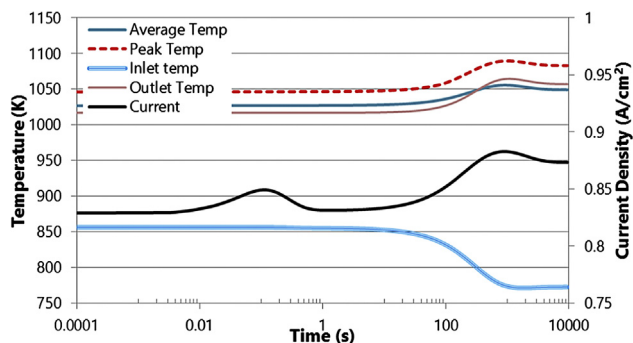Fig. 11 – Fuel cell system response to a step power demand increase.

Fig. 12 – Fuel cell system response to a step increase in fuel flow (10%).

temperature. The amount of heating that occurs along the cathode channel (the difference between inlet and outlet temperature in the figure) at this higher power output is 50% greater, causing significant increases in cell temperature gradients.

Despite the increased power demand and corresponding voltage reduction, the overall system efficiency rises due to the increased fuel utilization, but the increased temperature and temperature gradients are likely detrimental to long term operation and therefore not maintainable. The controlled response would initially behave similarly, but an increase in air flow would avoid the eventual rise in operating temperature. Fig. 11 showed the thermal transients occurring on the order of 100 s, which should allow sufficient time to modify the air blower flow rate. The additional air flow may exceed the heating rate of the pre-heater causing a slight drop in operating temperature. This can be overcome in a system with variable cathode recirculation by increasing cathode recirculation.

The second perturbation was an increase in fuel flow of 10%. It takes a short period before the fuel reaches the fuel cell, at which point the additional hydrogen causes a slight increase in current and the additional reformation causes a slight decrease in the cell outlet temperature. Very quickly thereafter the additional fuel is oxidized, increasing the heat recovered in the preheater and raising the cell operating temperature. The cell temperature continues to rise, reducing Ohmic losses and raising the current density, until the additional power output reduces the energy available for pre-heating back to steady-state levels. The higher fuel flow reaches a new equilibrium at a higher power output, current density and operating temperature. The increased current density causes steeper internal temperature gradients, which may not be sustainable. Fig. 12 demonstrates an interesting aspect of fuel cell technology, the potential to perform above design power output conditions for several minutes by simply increasing fuel flow. Novel dynamic control of the fuel utilization factor could manipulate fuel flow for dynamic operational benefit. Applied in a load following scenario with very short duration peak power demands, this feature would allow a system to be undersized by as much as 30% and still meet the peak demand for several minutes before significant temperature rise or changes occurred that might jeopardize stack durability. This "power boost" feature comes with a significant
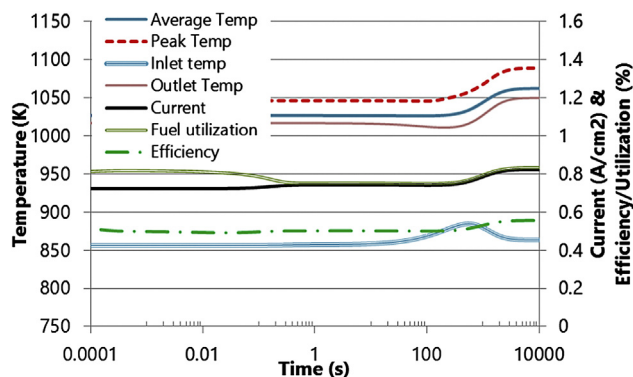
loss of efficiency, but would be expected to only rarely be employed for short duration peak demands.

Results of the third perturbation, a 10% reduction of the air flow rate, are presented in Fig. 13. This perturbation resulted in an immediate rise in the cathode inlet temperature and a subsequent heating of the fuel cell. Once again a new equilibrium was reached once the additional power produced by the fuel cell reduced the available energy for pre-heating the air. Thus, the inlet temperature was restored to steady state, but the average, peak, and outlet temperature of the fuel cell rose substantially with the additional internal power and heat generation.

The fourth perturbation was a sudden change in fuel composition from natural gas to a 90–10 natural gas-hydrogen blend. Results from this perturbation shown in Fig. 14 indicates that despite the higher hydrogen content in the raw fuel, the reformation yields less hydrogen and causes a small initial reduction in the current. Subsequently, the lower electrochemical heating in the stack reduced the energy available for pre-heating the air and decreased the operating temperature of the fuel cell. The lower temperature increased Ohmic polarization and further reduced the current and stack power. A new equilibrium was reached at substantially lower power and operating temperature. Control of the fuel flow rate or air flow will be necessary to compensate for any fuel blending or dynamic perturbation of fuel composition of this type.
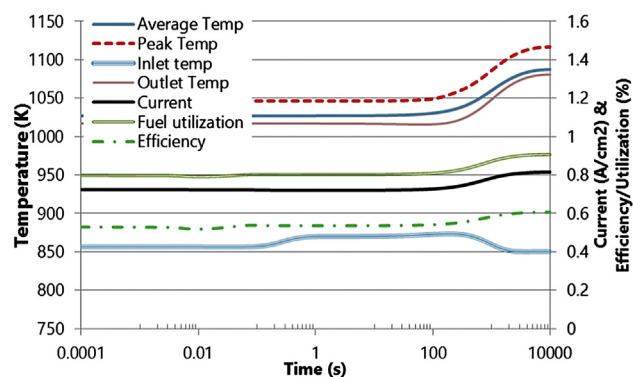

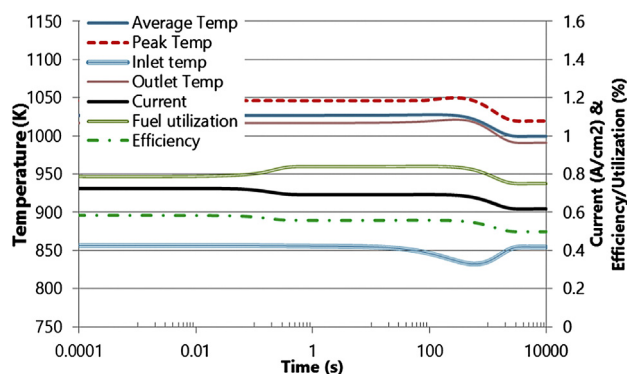Fig. 13 – Fuel cell system response to a step reduction in air flow of 10%.

Fig. 14 — Fuel cell system response to a step change in fuel composition.

The perturbations investigated each impact the open-loop FC response differently, but each can be independently controlled with specific controllers that manipulate certain variables. Systems with a variable cathode recirculation loop provide an additional manipulated variable for use in control systems. Cathode recirculation can rapidly adjust the inlet temperature, avoiding some of the large thermal deviations presented in the open-loop responses above. Cathode recirculation is beneficial from a controls perspective, though it may increase mechanical complexity and reduce nominal efficiency slightly.

The current analyses also apply to other HT-FC configurations such as hybrid fuel cell gas turbine (FC/GT) systems. As a result, cathode recirculation should be considered as a means of control for hybrid systems as well. Having previously determined system behavior and response, a central control strategy can achieve the operating constraints of temperature, thermal gradients, and fuel starvation during a load, fuel, or ambient condition perturbation by controlling voltage, air flow, fuel flow, and/or cathode recirculation.

7.   Conclusions

A unique dynamic model for high temperature fuel cell systems that captures the physics of air and fuel manifold heat transfer was developed from first principles and found to exhibit expected system level behavior. The readily calibrated model accurately captures the dynamic performance of both planar SOFC and MCFC systems of various sizes and flow configurations with a significant range of spatial resolution available. The amount of internal vs. external reformation has a different impact on cross and co-flow geometries. Higher spatial resolutions in modeling efforts will likely lead to more accurate simulations that identify the precise locations of the most severe thermal gradients for any particular flow geometry considered.

Design insights garnered from the steady-state analyses can be applied to the design of SOFC systems and hybrid FC/GT systems. The fuel to air ratio was shown to closely correlate with efficiency, and should be optimized in any design. Internal pre-heating, the novel physics of air and fuel manifold heat transfer physics captured in this study, shows a

dependence solely upon air flow rate (for a given stack design) regardless of other operational conditions. This is due to conduction limited internal heat mobility within the stack and spatial temperature gradients in the stack that are determined by the material set design and conductive properties. The importance of PEN temperature gradient as a control parameter cannot be overstated, and was found to depend significantly upon power density, inlet temperature, and air flow rate. MCFC systems responded favorably to increases in carbon dioxide concentration and fuel hydration for moderate steam-to-carbon ratios. Transient responses emphasized the drastically different time scales associated with electrochemical performance and cell thermal dynamics. Novel control strategies have the potential to make use of the intermediate time scales for rapid transient response of a fuel cell system with minimal cell thermal fluctuations. Dynamic responses to step perturbations verified the utility of the model for future integration and dynamic control development and analysis work for high temperature fuel cell and hybrid fuel cell gas turbine systems. Detailed physical models must be employed to study system level transient responses and determine the delicate balance between performance and longevity under dynamic operating conditions.

REFERENCES

[1] DOE Fuel Cell Technologies Program. Highlights from U.S. Department of Energy's fuel cell Recovery act Projects 2012. DOE/EE-0749.
[2] U.S. Department of energy office of energy efficiency & renewable energy. 2010 fuel cell technologies market report. U.S. Department of Energy; 2011. DOE/GO-102011—3296.
[3] U.S. Department of energy office of energy efficiency & renewable energy. Renewable energy generation 2012. DOE/GO-102012—3640.
[4] Energetics Incorporated. Fuel cells for buildings and stationary applications roadmap workshop 2002. [College Park].
[5] Hengeveld DW, Revankar ST. Economic analysis of a combined heat and power molten carbonate fuel cell system. Journal of Power Sources February 2007;165:300—6.
[6] Cheekatamarla PK, Finnerty CM, Robinson CR, Andrews SM, Brodie JA, Lu Y, et al. Design, integration and demonstration of a 50 W JP8/kerosene fueled portable SOFC power generator. Journal of Power Sources September 2009;193:797—803.
[7] Marra D, Bosio B. Process analysis of 1 MW MCFC plant. International Journal of Hydrogen Energy January 2007;32:809—18.
[8] Rashidi R, Berg P, Dincer I. Performance investigation of combined MCFC system. Journal of Hydrogen Energy 2009;1—11.

[9] Bove R, Lunghi P. Experimental comparison of MCFC performance using three different biogas types and methane. Journal of Power Sources August 2005;145:588–93.

[10] Greppi P, Bosio B, Arato E. Feasibility of the integration of a molten carbonate fuel-cell system and an integrated gasification combined cycle. International Journal of Hydrogen Energy October 2009;34:8664–9.

[11] Xu J, Froment GF. Methane steam reforming, methanation and water-gas shift: I. Intrinsic kinetics. AIChE Journal January 1989;35(1):88–96.

[12] Lukas MD, Lee KY, Ghezel-Ayagh H. Development of a stack simulation model for control study on direct reforming molten carbonate fuel cell power plant. Paper presented at. IEEE Power Engineering Society; 1999.

[13] Lukas MD, Lee KY, Ghezel-Ayagh H. Operation and control of direct reforming fuel cell power plant. Paper presented at. IEEE Power Engineering Society; 2000.

[14] Nakajo A. Thermomechanical and electrochemical degradation in anode-supported solid oxide fuel cell stacks. Lausanne: Ecole Polytechnique Federal de Lausanne; 2011.

[15] Sheng M, Mangold M, Kienle A. A strategy for the spatial temperature control of a molten carbonate fuel cell system. Journal of Power Sources Septempber 2006;162:1213–9.

[16] Brouwer J, Jabbari F, Leal EM, Orr T. Analysis of a molten carbonate fuel cell: numerical modeling and experimental validation. Journal of Power Sources November 2005;158:213–24.

[17] Greppi P, Bosio B, Arato. E. A steady-state simulation tool for MCFC systems suitable for on-line systems. International Journal of Hydrogen Energy 2008;33:6327–38.

[18] Fergus JW. Electrolytes for solid oxide fuel cells. Journal of Power Sources November 2006:30–40.

[19] Campanari S, Iora P. Definition and sensitivity analysis of a finite volume SOFC model for a tubular cell geometry. Journal of Power Sources 2004;132:113–26.

[20] Klein JM, Bultel Y, Georges S, Pons M. Modeling of a SOFC fuelled by methane: from direct internal reforming to gradual internal reforming. Chemical Engineering Science 2007:1636–49.

[21] Santin M, Traverso A, Magistri L. Liquid fuel utilization in SOFC hybrid systems. Applied Energy 2009:2204–12.

[22] Kim S, Yoon S, Bae J, Yoo YS. Performance analysis of CH4 driven SOFC short stack. Paper presented at. In: Proceedings of fuel cell 2009 2009. [Newport Beach].

[23] Costamagna P, Selimovic A, Borghi MD, Agnew G. Electrochemical model of the integrated planar solid oxide fuel cell (IP-SOFC). Chemical Engineering Journal 2004:61–9.

[24] Gariglio M, Benedictis F, Santurelli M. Experimental activity on two tubular solid oxide fuel cell cogeneration plants in a real industrial environment. International Journal of Hydrogen Energy 2009:1–8.

[25] Wolfgang W, Lorenz H. Design studies of mobile applications with SOFC-heat engine modules. Journal of Power Sources April 2002;106:338–43.

[26] Mueller F, Brouwer J, Jabbari F, Samuelsen S. Dynamic simulation of an integrated solid oxide fuel cell system including current-based fuel flow control. Transactions of the ASME May 2006:144–53.

[27] Xi H, Sun J, Tsourapas V. A control oriented low order dynamic model for planar SOFC using minimum Gibbs free energy method. Journal of Power Sources 2007:253–66.

[28] Sorrentino M, Pianese C. Control oriented modeling of solid oxide fuel cell auxiliary power unit for transportation applications. Journal of Fuel Cell Science and Technology 2009:041011–22.

[29] Achenbach E, Riensche E. Methane/steam reforming kinetics for solid oxide fuel cells. Journal of Power Sources 1994:283–8.

[30] Kaneko T, Brouwer J, Samuelsen GS. Power and temperature control of fluctuating biomass gas fueled solid oxide fuel cell and micro gas turbine hybrid system. Journal of Power Sources 2006:316–25.

[31] Mueller F, Jabbari F, Brouwer J, Roberts R, Junker T, GAH. Control design for a bottoming solid oxide fuel cell gas turbine hybrid system. Journal of Dynamic Systems, Measurement, and Control 2009:1–9.

[32] Roberts R, Brouwer J, Jabbari F, Junker T, Ghezel-Avagh H. Control design of an atmospheric solid oxide fuel cell/gas turbine hybrid system: variable versus fixed speed gas turbine operation. Journal of Power Sources 2006:484–91.

[33] Ghezel-Ayagh H. Multi_megawatt direct fuel cell/gas turbine product development. Paper presented at. In: International colloquium on environmentally preferred advanced power generation 2009. [Newport Beach].

[34] Lee SY, Kim DH, Lim HC, Chung GY. Mathematical modeling of a molten carbonate fuel cell (MCFC) stack. International Journal of Hydrogen Energy 2010;35:13096–103.

[35] Koh JH, Kang BS, Lim HC. Effect of various stack parameters on temperature rise in molten carbonate fuel cell stack operation. Journal of Power Sources 2000;91:161–71.

[36] Lin CK, Chen TT, Chyou YP, Chiang LK. Thermal stress analysis of a planar SOFC stack. Journal of Power Sources 2007;164:238–51.

[37] Qu Z, Aravind PV, Boksteeen SZ, Dekker NJJ, Jannsen AHH, Woudstra N, et al. Three-dimensional computational fluid dynamics modeling of anode-supported planar SOFC. International Journal of Hydrogen Energy 2011;36:10209–20.

[38] Thijssen JHJS. The impact of scale-up and production volume on SOFC manufacturing cost. National Energy Technology Laboratory; 2007.

[39] Surdoval W. The solide state energy conversion alliance (SECA). National Energy Technology Laboratory; 2001.

[40] Sugiura K, Matsuoka H, Tanimoto K. MCFC performance diagnosis by using the current-pulse method. Journal of Power Sources 2005;145:515–25.

[41] Aguiar P, Adjiman CS, Brandon NP. Anode-supported intermediate-temperature direct internal reforming solid oxide fuel cell: II. Model-based dynamic performance and control. Journal of Power Sources 2005;147:136–47.

[42] Stiller C, Thorud B, Bolland O, Kandepu R, Imsland L. Control strategy for a solid oxide fuel cell and gas turbine hybrid system. Journal of Power Sources 2005;158:303–15.

[43] Sorrentino M, Pianese C. Model-based development of low-level control strategies for transient operation of solid oxide fuel cell systems. Journal of Power Sources 2011;196:9036–45.

[44] Mueller F, Gaynor R, Auld AE, Brouwer J, Jabbari F, Samuelsen GS. Synergistic integration of a gas turbine and solid oxide fuel cell for improved transient capability. Journal of Power Sources 2008;176:229–39.

[45] Leucht F, Bessler WG, Kallo J, Friedrich KA, Muller-Steinhagen H. Fuel cell system modeling for solid oxide fuel cell/gas turbine hybrid power plants, part I: modeling and simulation framework. Journal of Power Sources 2011;196:1205–15.

[46] Li M, Rao AD, Samuelsen GS. Performance and costs of advanced sustainable central power plants with CCS and H2 co-production. Applied Energy 2012;91(1):43–50.